Supporting Information for

The Unpoppable Bubble: Suppressing Drainage-induced Rupture through Vibration

Weikang Lin[1†], Jigang Feng[2†], Yunfei Liu[2,3†], Yi Zheng[1†], Xiaodan Yang[1], Qiqi Pan[1], Zhaoye Qin[2*], Dominic Vella[3*], Zhengbao Yang[1*]

[1]Department of Mechanical and Aerospace Engineering, Hong Kong University of Science and Technology, Clear Water Bay, Hong Kong, China
[2]State Key Laboratory of Tribology, Department of Mechanical Engineering, Tsinghua University, Beijing, China
[3]Mathematical Institute, University of Oxford, Oxford OX2 6GG, United Kingdom

* Zhaoye Qin[2*], Dominic Vella[3*], Zhengbao Yang[1*]

Email: zbyang@ust.hk; dominic.vella@maths.ox.ac.uk; qinzy@mail.tsinghua.edu.cn
[†]These authors contributed equally to this work.

This PDF file includes:

1. Double spring-mass model for the vibration bubble system

The presence of the bubble within a sessile drop modifies the amplitude-frequency response of the system: compared with the droplet-only case, the vibration intensity of the platform is markedly suppressed. To capture this difference, we model the system as a double mass spring system with spring stiffnesses K_i and masses m_i (*i* = 1, 2), as defined in Fig. S3A.

Before the initiation of a bubble, the system consists of a sessile droplet partially wetting a planar solid support, which is vertically vibrated at a frequency of $\omega/2\pi$ with an amplitude *A*. The vibration attenuation characteristics of the sessile droplet system are illustrated in Fig. S3B, showing that m_1 and m_2 are effectively connected by a rigid spring, $K_2 = \infty$, and the system behaves as a single-degree-of-freedom (SDOF) oscillator(1). For the sessile droplet system, the differential equation of motion can then be expressed as: $m\ddot{x} + C_1\dot{x} + K_1x = F_0 \sin \omega t$. The displacement of the droplet satisfies $x = X \sin(\omega t - \varphi)$, where $X,\ \omega,\ \varphi$ represent the amplitude, angular frequency, and phase of the forcing, respectively. Thus, the amplitude of the forced vibration can be calculated as:

$$X = \frac{F_0}{\sqrt{(K_1 - m\omega^2)^2 + (C_1\omega)^2}} \quad [1]$$

As shown in Fig. S3C, the vibration of the system no longer decays at a single frequency once a bubble is introduced into the droplet. However, the double mass spring system is able to account for this by dividing the system into two parts: the platform with m_1, K_1, C_1, as the primary system and the bubble with m_2, K_2, C_2 as the damper.

$$m_1\ddot{x}_1 + (C_1 + C_2)\dot{x}_1 - C_2\dot{x}_2 + (K_1 + K_2)x_1 - K_2x_2 = F_1e^{i\omega t} \quad [2]$$

$$m_2\ddot{x}_2 - C_2\dot{x}_1 + C_2\dot{x}_2 - K_2x_1 + K_2x_2 = 0 \quad [3]$$

The displacement of the platform and the bubble can be expressed as:

$$x_1(t) = X_1\mathrm{e}^{\mathrm{i}(\omega t - \varphi)} \quad [4]$$

$$x_2(t) = X_2\mathrm{e}^{\mathrm{i}(\boldsymbol{\omega} t - \boldsymbol{\varphi})} \quad [5]$$

Given that the damping C_1 is relatively low and can be neglected, the formulation can be simplified to:

$$\begin{bmatrix} K_1 + K_2 - \omega^2 m_1 + \mathrm{i}\omega C_2 & -(K_2 + \mathrm{i}\omega C_2) \\ -(K_2 + \mathrm{i}\omega C_2) & K_2 - \omega^2 m_2 + \mathrm{i}\omega C_2 \end{bmatrix} \begin{bmatrix} X_1\mathrm{e}^{-\mathrm{i}\varphi} \\ X_2\mathrm{e}^{-\mathrm{i}\varphi} \end{bmatrix} = \begin{bmatrix} F_1 \\ 0 \end{bmatrix} \quad [6]$$

The solutions for X_1 and X_2 are as follows:

$$X_1 = F_1\sqrt{\frac{(K_2 - \omega^2 m_2)^2 + \omega^2 {C_2}^2}{[(K_1 - \omega^2 m_1)(K_2 - \omega^2 m_2) - \omega^2 K_2 m_2]^2 + \omega^2 {C_2}^2 (K_1 - \omega^2 m_1 - \omega^2 m_2)^2}} \quad [7]$$

$$X_2 = F_1\sqrt{\frac{K_2^2 + \omega^2 {C_2}^2}{[(K_1 - \omega^2 m_1)(K_2 - \omega^2 m_2) - \omega^2 K_2 m_2]^2 + \omega^2 {C_2}^2 (K_1 - \omega^2 m_1 - \omega^2 m_2)^2}} \quad [8]$$

The resulting expression for the response amplitude can be written in dimensionless terms as follows:

$$x_{1\mathrm{d}} = \frac{X_1}{X_{1s}} = \sqrt{\frac{(a^2 - \lambda^2) + (2\xi\lambda)^2}{(1 - \lambda^2)(a^2 - \lambda^2) - \beta(a\lambda)^2 + (2\xi\lambda)^2(1 - \lambda^2 - \beta\lambda^2)^2}} \quad [9]$$

where, $X_{1s} = \frac{F_1}{K_1}$, $\beta = \frac{m_2}{m_1}$, $\alpha = \frac{\omega_2}{\omega_1}$, $\lambda = \frac{\omega}{\omega_1}$, and m_1 and m_2 represent the mass of the platform and bubble, respectively. Experiments results (Fig. 3B of the main paper) show that the bubble film thickness follows $h \propto R^{-2}$, therefore, the mass of the bubble m_2 remains almost unchanged.

From our experimental results, we are able to fit $\beta = 1/40$, and $\xi = 0.025$. ω_1 and ω_2 are the natural frequency of the platform and bubble, respectively, and are measured through the free decay test (Fig. S3B and *C*). Repeating the free-decay test for different bubble volumes yields ω_1 and ω_2, as summarized in Fig. S3D. Based on these measured frequencies, the dimensionless frequency ratios α and λ are then calculated and plotted as functions of bubble volume in Fig. S3E.

The theoretical curve for the platform's displacement x_1 can be obtained from the above expressions, as shown in Fig. S3F, matching the trend observed in the experimental data.

2. Dynamic analysis of the sessile bubble system

2.1 Model Formulation and Governing Equations

2.1.1. Physical Setup

Accounting for the liquid retained in the basal meniscus by gravity, we consider a spherical bubble of radius R bounded by a thin film of effective volume V_0. The liquid is characterized by its density ρ and dynamic viscosity μ. We employ a spherical coordinate system (r, θ, φ), with the apex (north pole) of the bubble at $\theta = 0$ (Fig. 3A). The analysis is restricted to the upper hemisphere where the film exists. A core assumption is that the film thickness h, is much smaller than the bubble radius, $h \ll r$, allowing for a significant simplification of the fluid dynamics.

2.1.2. Kinematic Constraint: Fixed Film Volume

The total volume of the liquid film is conserved. For a thin film covering the upper hemisphere, this is expressed as $V_0 \approx 2\pi R^2 h$ and $h = \frac{K_v}{R^2}$. Where $K_v = \frac{V_0}{2\pi}$ is a constant determined by the initial conditions. This geometric constraint is fundamental to the non-linear behavior of the system.

The film thickness *h* is important when studying the stability of the bubble. Following McEntee and Mysels(2), the thickness of the bubble is measured via the Taylor-Culick velocity measurement: A hole in a punctured bubble film grows because of unbalanced surface tension forces at the edge of the hole. The speed at which the hole grows, v, is related to the thickness h via $h = \frac{2\sigma}{\rho v^2}$. As shown in Fig. 3B of the main paper, the vibration intensity shows no significant influence on the bubble thickness; the bubble thickness is only determined by its size *r*, showing the relationship of $h \propto R^{-2}$, consistent with our previous assumption of conserved liquid volume within the film.

2.1.3. Governing Momentum Equation

The system is subjected to a constant gravitational acceleration, g, and a vertical sinusoidal vibration, $\boldsymbol{a}_{\text{vib}}(t) = -A\omega^2 \cos\omega t \ \hat{\boldsymbol{z}}$, where A and ω are the vibration amplitude and angular frequency, respectively. In a reference frame that is moving with the plate, the fluid experiences an effective time-dependent gravitational acceleration:

$$g_{\text{eff}}(t) = g\left(1 + \frac{A\omega^2}{g}\cos\omega t\right) = g(1 + \Gamma\cos\omega t) \qquad \textbf{[10]}$$

where $\Gamma = \frac{\mathrm{A}\omega^2}{g}$is the dimensionless vibration amplitude and compares the strength of the vibration-induced acceleration with that due to gravity.

Projecting along the surface tangent gives the tangential body force per unit mass

$$g_s(t) = g_{\text{eff}}(t)\sin\theta = g(1 + \Gamma\cos\omega t)\sin\theta \qquad \textbf{[11]}$$

The motion of the fluid film is governed by the unsteady Navier-Stokes (NS) equations. In the spherical polar coordinates that are most natural here, and assuming there is no variation in the azimuthal, i.e. ϕ, direction we have that the fluid velocity (u, v) satisfies incompressibility

$$\frac{1}{r^2}\frac{\partial}{\partial r}(r^2 v) + \frac{1}{r^2\sin\theta}\frac{\partial}{\partial\theta}(\sin\theta\ u) = 0 \qquad \textbf{[12]}$$

with the momentum equation in the meridional direction

$$\frac{Du}{Dt} + \frac{uv}{r} = -\frac{1}{\rho\, r}\frac{\partial p}{\partial\theta} + \nu\left[\frac{1}{r^2}\frac{\partial}{\partial r}\left(r^2\frac{\partial u}{\partial r}\right) + \frac{1}{r^2}\frac{\partial}{\partial\theta}\left(\frac{1}{\sin\theta}\frac{\partial(u\sin\theta)}{\partial\theta}\right) + \frac{2}{r^2}u\right] + g(1 + \Gamma\cos\omega t)\sin\theta \qquad \textbf{[13]}$$

where $\nu = \mu/\rho$ is the kinematic viscosity. (Following van der Schaaf and Beerkens(3), we focus on the meridional velocity – the radial velocity can be inferred from incompressibility since gradients in the pressure p are small.)

Ordinarily(4, 5), bubble drainage is modelled as occurring with stress free boundary conditions, which leads to extensional flow within the film. In this problem, we believe the interface to be effectively immobilized by a

streaming flow within the air outside the bubble. This induces an effective no-slip boundary condition on this interface and means that making the usual thin-film approximation(6), $h \ll R$, the tangential component of the NS equation reads

$$\left(\frac{\partial u}{\partial t} + u\frac{\partial u}{\partial s} + v\frac{\partial u}{\partial y}\right) = -\frac{1}{\rho}\frac{\partial p}{\partial s} + \nu\frac{\partial^2 u}{\partial y^2} + g_s(t) \qquad \textbf{[14]}$$

where $s = R\theta$ and $y = r - R$ are local coordinates and $u(s,y,t)$ and $v(s,y,t)$ are the tangential and normal velocity components, respectively.

To determine the dominant balance of forces, we introduce the Stokes number (*Stk*), defined as the ratio of unsteady inertia to viscous shear forces:

$$Stk \equiv \frac{\left(\rho\frac{\partial}{\partial t}u\right)}{\left(\mu\frac{\partial^2}{\partial y^2}u\right)} \approx \frac{\left(\rho\frac{1}{\frac{1}{\omega}}u\right)}{\left(\mu\frac{1}{h^2}u\right)} = \frac{\omega h^2}{\nu} \qquad \textbf{[15]}$$

(Note that the Stokes number can be interpreted as the square of the film thickness relative to the Stokes length $\ell_s = \left(\frac{\nu}{\omega}\right)^{1/2}$.)

Substituting the volume constraint $h = \frac{K_v}{R^2}$, we uncover the critical dependence of the system's physics on the bubble radius:

$$Stk = \frac{\omega K_v^2}{\nu} R^{-4} \qquad \textbf{[16]}$$

This strong dependence indicates that as the bubble size *R* increases, the flow regime transitions dramatically from an inertia-dominated regime ($Stk \gg 1$) to a viscosity-dominated regime ($Stk \ll 1$). (While this may initially seem counter-intuitive, we emphasize that this is because of the change in thickness that accompanies a change in radius at fixed fluid volume within the film.) We find that a typical value for the critical radius $R_c = \left(\frac{\omega K_v^2}{\nu}\right)^{1/4}$ (which separates the inertia-dominated and viscosity-dominated regimes) is $R_c = 6.45\ mm$.

We introduce dimensionless parameters as follows:

$$\tau = \omega t,\ \ Y = y/h,\ \ S = s/R,\ \ U = u/u_e,\ \ \Omega = \omega/\left(\frac{g}{R}\right)^{1/2} \qquad \textbf{[17]}$$

where $u_e = \frac{gh^2}{\nu} = \left(\frac{g}{\omega}\right) Stk$, i.e. the drainage velocity with immobilized interfaces(7), is defined as the natural velocity scale.

In this model, the thin-film limits are considered here, and the dynamics are dominated by the tangential gravitational drainage, allowing us to neglect the minor capillary pressure gradients ($\partial p/\partial s$) and the normal advective transport terms ($v\partial u/\partial y$). Therefore, the NS equation in Eq.[14] can be expressed in dimensionless form as

$$Stk\frac{\partial U}{\partial \tau} + Stk^2\Omega^{-2}U\frac{\partial U}{\partial S} = \frac{\partial^2 U}{\partial Y^2} + (1 + \Gamma\cos\tau)\sin\theta \qquad \textbf{[18]}$$

2.2. The Viscous Regime (Large *R*, $Stk \ll 1$)

For large bubble radii *R*, the constraint of conserved liquid volume forces the film thickness *h* to decrease sharply. This geometric change causes the value of *Stk* to decrease significantly. Consequently, for large *R*, the system enters a viscosity-dominated regime ($Stk \ll 1$) where the fast oscillatory motion does not drive an inertial response in the fluid. In this limit, the profile of the oscillatory flow is governed by viscous forces and adopts a parabolic shear flow morphology.

To resolve the hierarchy of forces acting on the thin film, we perform a perturbation analysis. We expand the dimensionless fluid velocity field *U* in powers of the vibration amplitude Γ:

$$U(\tau,Y,S) = U_0(Y,S) + \Gamma U_1(\tau,Y,S) + \Gamma^2 U_2(\tau,Y,S) \qquad \textbf{[19]}$$

where U_0 is the zeroth-order, steady-state flow driven by the mean gravitational force, responsible for the drainage flux; U_1 is the first-order, oscillatory flow driven by the time-varying component of the external forcing; U_2 is the second-order flow, known as the steady streaming or rectified flow. It is driven by the non-linear self-interaction of the first-order flow and is responsible for the stabilizing pumping flux. (Note that the value of Γ is typically large in experiments, and so the power series in (19) can converge only if $\Gamma_2^{2U} \ll \Gamma U_1$ etc.)

Substituting the above equation into the dimensionless NS equation in Eq. [18] and collecting terms order by order in Γ, we can get

$$[\Gamma^0]: \frac{Stk^2}{\Omega^2} U_0 \frac{\partial U_0}{\partial S} = \frac{\partial^2 U_0}{\partial Y^2} + \sin\theta \quad \textbf{[20]}$$

$$[\Gamma^1]: Stk \frac{\partial U_1}{\partial \tau} + \frac{Stk^2}{\Omega^2}(U_0 \frac{\partial U_1}{\partial S} + U_1 \frac{\partial U_0}{\partial S}) = \frac{\partial^2 U_1}{\partial Y^2} + \cos\tau \sin\theta \quad \textbf{[21]}$$

$$[\Gamma^2]: Stk \frac{\partial U_2}{\partial \tau} + \frac{Stk^2}{\Omega^2}(U_0 \frac{\partial U_2}{\partial S} + U_1 \frac{\partial U_1}{\partial S} + U_2 \frac{\partial U_0}{\partial S}) = \frac{\partial^2 U_2}{\partial Y^2} \quad \textbf{[22]}$$

2.2.1 Zeroth-Order: Gravitational Drainage (U_0)

At the zeroth order, inertial terms may be neglected. The flow is a steady drainage driven by the gravitational component tangential to the bubble surface. Eq.[20] can be reduced to

$$0 = \frac{\partial^2 U_0}{\partial Y^2} + \sin\theta \quad \textbf{[23]}$$

Due to the linearity of viscous dissipation within the confined film thickness, the steady velocity scales with the driving force, leading to a Poiseuille-like velocity scaling profile:

$$U_0 \sim \sin\theta \quad \textbf{[24]}$$

Integrating this scaling profile across the normalized dimensionless film thickness provides the characteristic scaling for the gravitational drainage flux Q_{drain}:

$$Q_{drain} = \int_0^1 U_0 \, dY \sim \sin\theta \quad \textbf{[25]}$$

2.2.2 First-Order: Linear Oscillation (U_1)

The first-order component is driven by the vibrational acceleration. Since $Stk \ll 1$, the unsteady inertia term is negligible compared to the viscous term. The flow responds quasi-steadily to the forcing in Eq.[21]:

$$0 = \frac{\partial^2 U_1}{\partial Y^2} + \cos\tau \sin\theta \quad \textbf{[26]}$$

The resulting oscillatory flow U_1 directly mirrors the periodic driving force:

$$U_1 \sim \sin\theta \cos\tau \quad \textbf{[27]}$$

2.2.3 Second-Order: Acoustic Streaming and Pumping (U_2)

At the second order, we focus on the time-averaged steady flow $\langle U_2 \rangle$ (hereafter denoted as U_2) which governs the stability against drainage. Applying the time-average operator $\langle \cdot \rangle = 1/2\pi \int_0^{2\pi} (\cdot)\, d\tau$ to Eq.[22], and ignoring the higher order small terms $(U_0 \, \partial U_2/\partial S + U_2 \, \partial U_0/\partial S)$, we find that:

$$\frac{\partial^2 U_2}{\partial Y^2} = \frac{Stk^2}{\Omega^2} \langle U_1 \frac{\partial U_1}{\partial S} \rangle \quad \textbf{[28]}$$

Substituting Eq.[27] into the right-hand side of Eq.[28], the inertial source term scales can be obtained as:

$$\frac{Stk^2}{\Omega^2} \langle U_1 \frac{\partial U_1}{\partial S} \rangle \sim \frac{Stk^2}{\Omega^2} \langle \cos^2\tau \rangle \sin\theta \frac{\partial(\sin\theta)}{\partial S} \sim \frac{Stk^2}{\Omega^2} \sin\theta \cos\theta \quad \textbf{[29]}$$

Then, we solve this differential equation in Eq. [28] as follows:

$$U_2 \sim \frac{Stk^2}{\Omega^2} \sin\theta \cos\theta \quad \textbf{[30]}$$

The total upward pumping flux is obtained by integrating the streaming velocity:

$$Q_{pump} = \int_0^1 \Gamma^2 U_2 \, dY \sim \Gamma^2 \frac{Stk^2}{\Omega^2} \sin\theta\cos\theta \quad \textbf{[31]}$$

2.2.4 Stability Threshold (Flux Balance)

The liquid film is stable when the upward pumping flux compensates for the downward drainage flux $|Q_{pump}| \geq |Q_{drain}|$. Substituting Eqs.[31] and [25]:

$$\Gamma^2 \frac{Stk^2}{\Omega^2} \sin\theta\cos\theta \gtrsim \sin\theta \quad \textbf{[32]}$$

Focusing on the critical region near the apex ($\cos\theta \approx 1$), and simplifying:

$$\Gamma^2 \gtrsim \frac{\Omega^2}{Stk^2} \quad \textbf{[33]}$$

By redefining the collective proportionality constant, this resolves cleanly into the final stability condition:

$$\Gamma_{viscous} \geq \frac{C_0}{Stk}\Omega \quad \textbf{[34]}$$

where C_0 is a dimensionless constant.

2.3. The Inertial Regime (Small R, $Stk \gg 1$)

For small bubbles ($Stk \gg 1$), the characteristic timescale for viscous momentum diffusion across the film is far greater than the period of the high-frequency vibration. In this limit, fluid inertia dominantly counterbalances the external vibrational forcing. From a scaling perspective, this indicates that the viscous dissipation terms can be neglected relative to the unsteady inertial terms when establishing the leading-order dynamics.

2.3.1 Flux Balance in the Inertial Limit

Under these conditions, the viscous terms in the NS equations vanish, reducing the dynamics to an unsteady Euler balance. The dimensionless NS equation in Eq. [18] becomes:

$$Stk\frac{\partial U}{\partial \tau} + \frac{Stk^2}{\Omega^2} U \frac{\partial U}{\partial S} = (1 + \Gamma\cos\tau)\sin\theta \quad \textbf{[35]}$$

To determine stability, we will compare the downward drainage flux driven by gravity against the upward pumping flux driven by the vibrational inertia. First, the gravitational drainage flux in this uniform flow regime scales directly with the gravitational component:

$$Q_{drain} \sim \sin\theta \quad \textbf{[36]}$$

For the dimensionless upward pumping flux, the oscillatory motion is first driven purely by the vibrational acceleration against fluid inertia, the NS equation in Eq. [35] can be reduced as follows:

$$U_1 = \frac{1}{Stk}\sin\tau \sin\theta \quad \textbf{[37]}$$

where we can find that the amplitude of oscillation scales inversely with the large Stokes number, reflecting high inertial resistance.

The stabilizing pumping effect arises from the time-averaged convective inertial term in the NS equation, and the inertial rectification drives a net mean streaming velocity. In spherical coordinates, the scaling of this convective interaction yields:

$$U_{pump} \sim \Gamma^2 \left\langle -Stk^2 U_1 \frac{\partial U_1}{\partial S} \right\rangle \sim \frac{\Gamma^2}{2\Omega^2}\sin\theta\cos\theta \quad \textbf{[38]}$$

Since the flow profile is uniform, the total upward pumping flux is simply the integration of this mean velocity, which is equivalent to the velocity itself in dimensionless form:

$$Q_{pump} = \int_0^1 U_{pump}\, dY \sim \frac{\Gamma^2}{2\Omega^2}\sin\theta\cos\theta \quad \textbf{[39]}$$

2.3.2 Stability Threshold (Flux Balance)

This upward pumping flux must overcome the drainage flux. The bubble remains stable against drainage when $Q_{pump} \geq Q_{drain}$, that is

$$\frac{\Gamma^2}{2\Omega^2}\sin\theta\cos\theta \geq \sin\theta \quad \textbf{[40]}$$

Focusing on the critical region near the bubble apex where thinning occurs ($\theta \to 0, \cos\theta \approx 1$), and thus the linear scaling law can be given by:

$$\Gamma_{inertial} \geq C_1\Omega \quad \textbf{[41]}$$

where C_1 is dimensionless constant.

2.4. Conclusion

Our theoretical analysis demonstrates that the stabilization of a liquid film on a vibrated bubble is governed by a crossover between two distinct physical regimes. The fundamental cause of this crossover is the fixed volume, which couples the system's geometry to its hydrodynamics via the Stokes number.

Stable Zone: The region satisfying both criteria ($\Gamma \geq \Gamma_{inertial}$ and $\Gamma \geq \Gamma_{viscous}$).

Unstable Zone: Where gravitational drainage exceeds maximum pumping capacity.

Metastable Transition Zone: The intersection region between the two scaling laws represents a regime crossover. Within this intermediate regime, unsteady fluid inertia and viscous dissipation are of comparable magnitude. The complex fluid responses lead to a sensitive, tightly matched competition between fluxes. Experimentally, this complexity translates to high sensitivity to perturbations and inherently metastable bubble lifetimes.

Figures

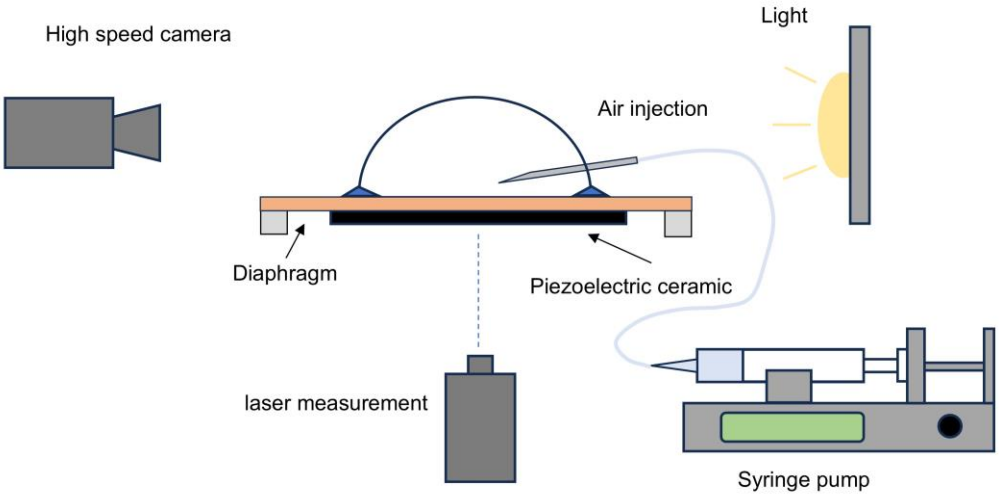

Fig. S1. Schematic illustration of the experimental setup of the bubble vibration platform. The setup includes a function generator (not shown), a piezoelectric actuator, a syringe pump, and a high-speed camera for analyzing interfacial dynamics.

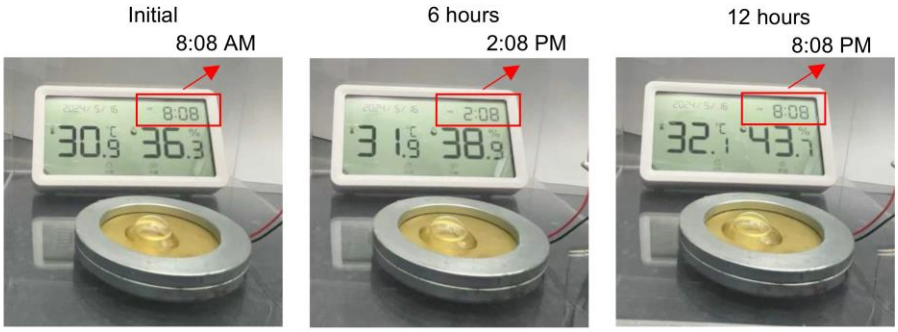

Fig. S2. Long-term stabilization of a bare bubble under vibration A bare bubble maintained stability for more than 12 hours in the presence of continuous mechanical vibration (From 8:08 AM to 8:08 PM.). Frames extracted from Supplementary Video 3.

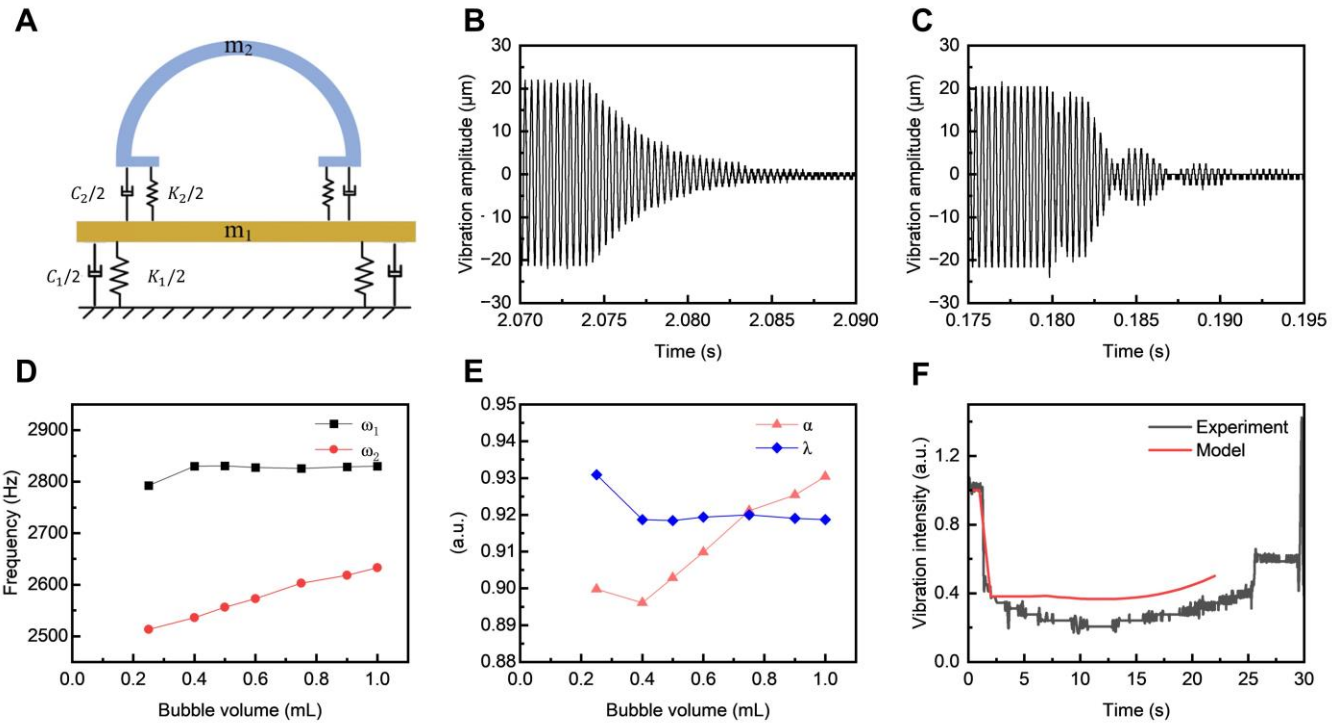

Fig. S3. Dynamic analysis of the bubble vibration system. (A) Schematic of the double-spring system depicting the bubble vibration system. **(B** and **C)**, The vibration damping characteristics of the sessile droplet system (B) and the bubble system (C) when subject to the free decay test. **(D)** The natural frequencies ω_1 and ω_2.of the system as functions of the bubble size. **(E)** The parameter $\alpha = \omega_2/\omega_1$ and $\lambda = \omega/\omega_1$ as functions of the bubble size. **(F)** Comparison of the predicted and measured evolution of the vertical amplitude of the bubble system. The experimental data (black line) are fitted by the double spring-mass model with fitting parameters (red line).

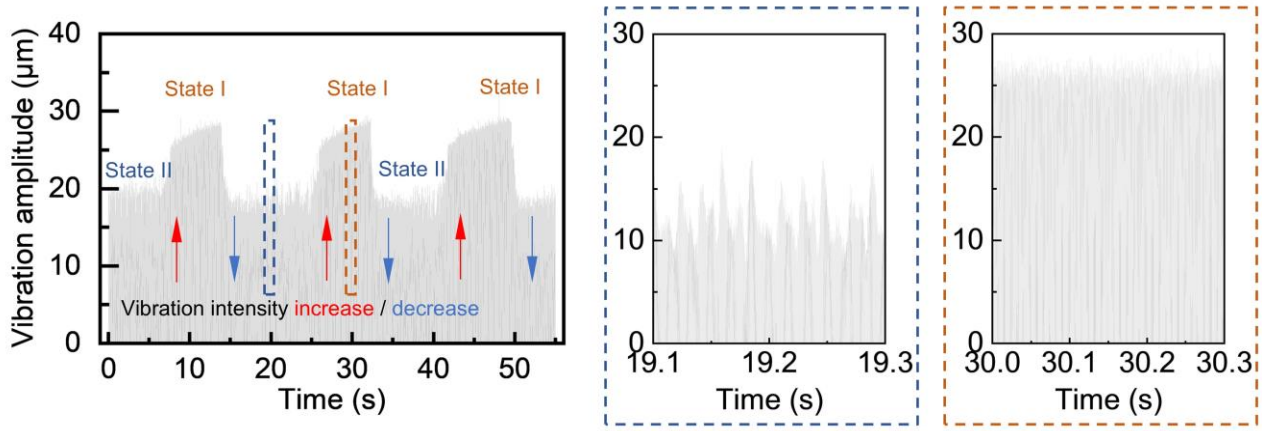

Fig. S4. Transition of the bubble state versus vibration intensity. The change of the vibration intensity leads to reversals in the state of the bubble. Increasing the vibration intensity promotes a change in the bubble state from the oscillation state (mode **II)** to the static state (mode **I)**.

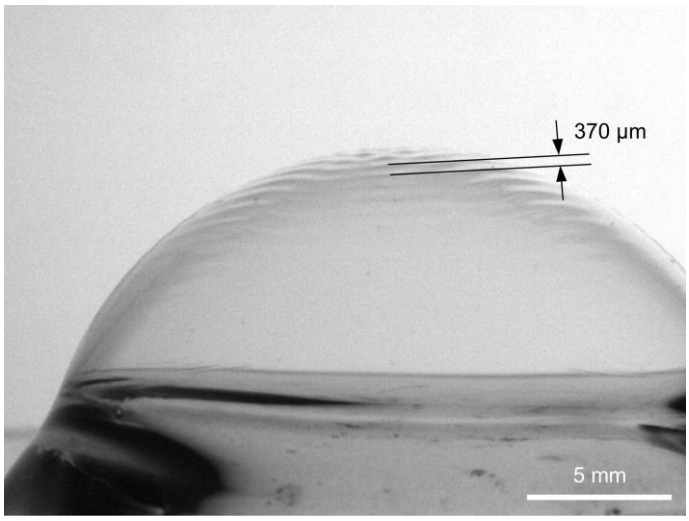

Fig. S5. Measurement of the capillary wave wavelength.

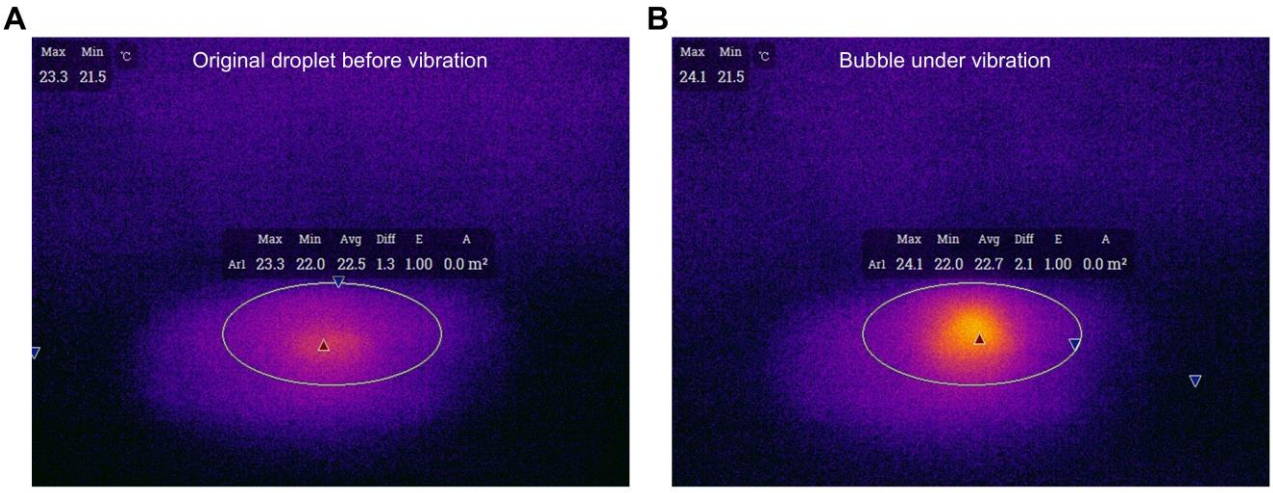

Fig. S6. Thermal imaging of the droplet and the bubble under vibration. (A) Original droplet before vibration. **(B)** Bubble formed under vibration.

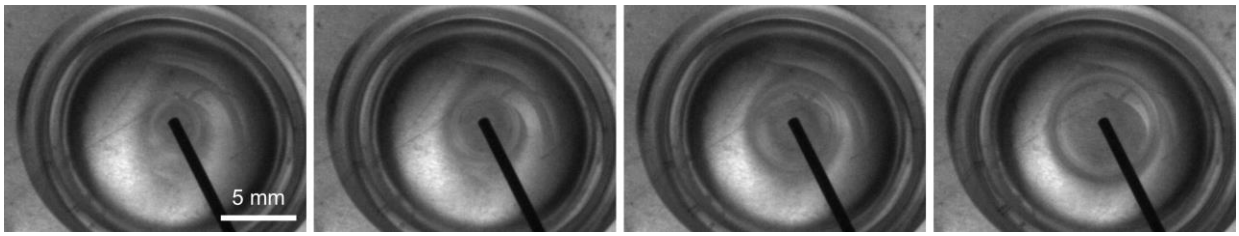

Fig. S7. Measurement of the bubble film thickness. High-speed imaging sequence showing the approach of a heated needle toward a stationary bubble (Static state I) under vibration conditions, and the resulting film rupture. Time interval between consecutive frames is 0.667 ms.

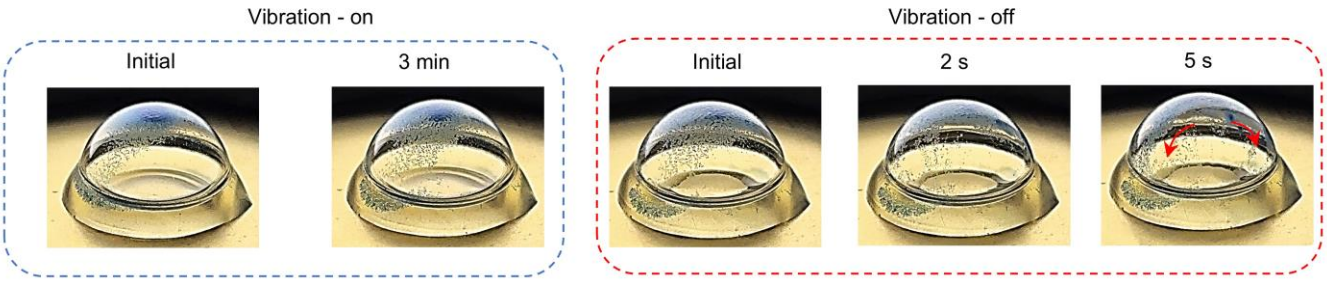

Fig. S8. Comparison of the bubble drainage with or without vibration. Note that in the vibrating state (left) the particles remain stable on the minute time scale; as soon as the vibration is turned off (right), particles very quickly fall down the bubble surface.

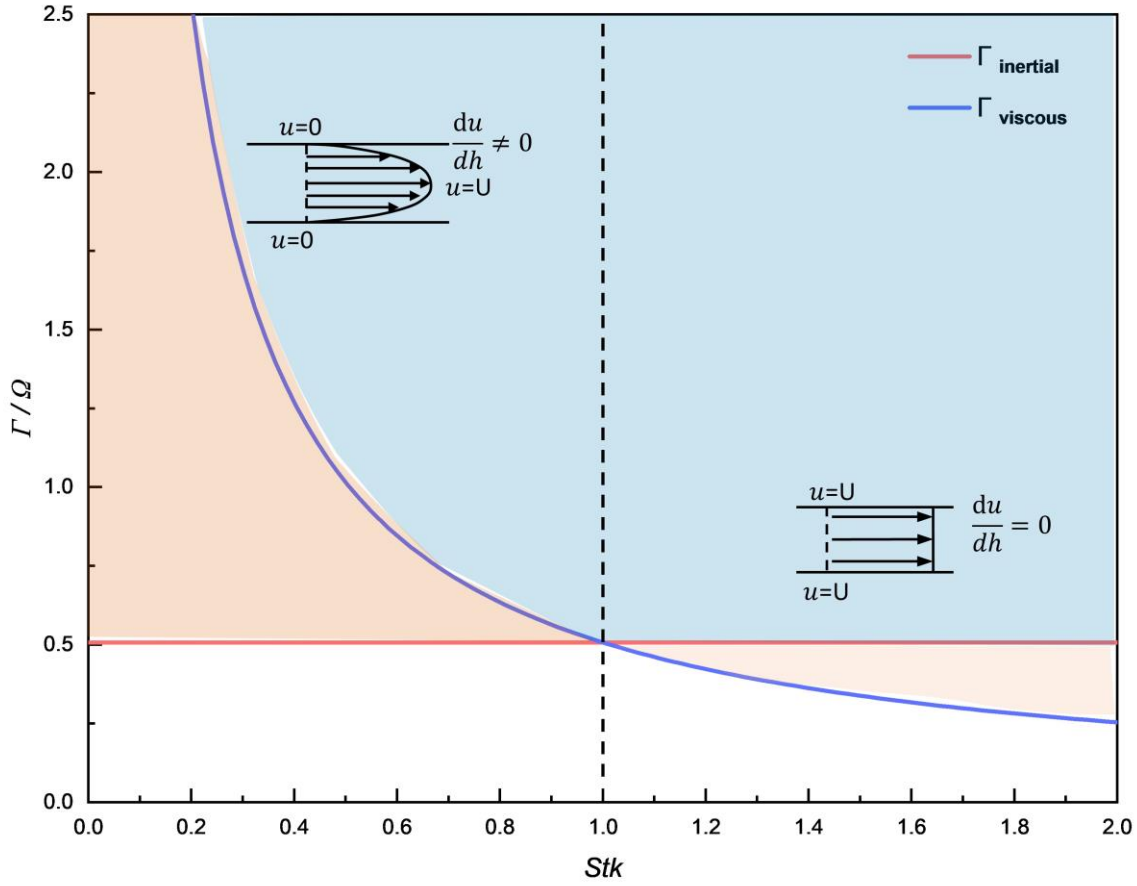

Fig. S9. Theoretical stability thresholds. The plot compares the critical vibration intensities for the inertial ($\Gamma_{inertial}$, red) and viscous ($\Gamma_{viscous}$, blue) regimes, intersecting at the crossover *Stk* = 1.

Movie S1. Bubble in natural state (without vibration) with continuous air injection
Movie S2. Bubble in static state (mode I) with continuous air injection
Movie S3. A bare bubble is stabilized for over 12 hours in the vibration condition
Movie S4. Bubble in oscillation state (mode II) with continuous air injection
Movie S5. Bubble in oscillation state (mode II) with intermittent air injection
Movie S6. Bubble state transition with the change of vibration intensity
Movie S7. Bubble in capillary wave state (mode III) with continuous air injection
Movie S8. Bubble in capillary wave state (mode III) with intermittent air injection
Movie S9. Puncture-proof bubble
Movie S10. Extreme deformation with a needle piercing horizontally
Movie S11. Demonstration of a stable bubble serves as a micro airtight reaction chamber

SI References

1. K. Sun, L. Shu, F. Jia, Z. Li, T. Wang, Vibration-induced detachment of droplets on superhydrophobic surfaces. *Phys. Fluids* **34** (2025).
2. W. R. Mcentee, W. R. Mcentee, K. J. Mysels, The bursting of soap films. I. An experimental study. *J. Phys. Chem.* **73**, 3018-3028 (1969).
3. J. van der Schaaf, R. G. C. Beerkens, A model for foam formation, stability, and breakdown in glass-melting furnaces. *J. Colloid Interface Sci.* **295**, 218–229 (2006).
4. P. D. Howell, The draining of a two-dimensional bubble. *J. Eng. Math.* **35**, 251–272 (1999).
5. C. Bartlett, A. T. Oratis, M. Santin, J. C. Bird, Universal non-monotonic drainage in large bare viscous bubbles. *Nat. Commun.* **14**, 1–7 (2023).
6. A. Oron, S. H. Davis, S. G. Bankoff, Long-scale evolution of thin liquid films. *Rev. Mod. Phys.* **69**, 931 (1997).
7. C. T. Nguyen, *et al.*, Film drainage and the lifetime of bubbles. *Geochem. Geophys. Geosyst.* **14**, 3616–3631 (2013).